Reactive Oxygen Species Formation and Peroxide and Carbonyl Decomposition in Aqueous Photolysis of Secondary Organic Aerosols

Lena Gerritz[1#], Jinlai Wei[1#], Ting Fang[1,2], Cynthia Wong[1], Alexandra L. Klodt[1], Sergey A. Nizkorodov[1,*], Manabu Shiraiwa[1,*]

[1] Department of Chemistry, University of California, Irvine, CA, 92697-2025, USA

[2]Sustainable Energy and Environment Thrust, The Hong Kong University of Science and Technology (Guangzhou), Nansha, Guangzhou, Guangdong, 511400, China.

# Equal contribution

* nizkorod@uci.edu;* m.shiraiwa@uci.edu

KEYWORDS

Particulate matter, photochemical aging, cloud processing, free radicals, high resolution mass spectrometry

SYNOPSIS

Oxidized organic compounds are ubiquitous in the atmospheric environment. Our experiments show that these compounds produce a variety of free radicals driving important aging processes for air pollutants.

To be submitted to *Environ. Sci. Technol.*

ABSTRACT

The mechanism and kinetics of reactive oxygen species (ROS) formation when atmospheric secondary organic aerosol (SOA) is exposed to solar radiation are poorly understood. In this study, we combined an *in-situ* UV-Vis irradiation system with electron paramagnetic resonance (EPR) spectroscopy to characterize the photolytic formation of ROS in aqueous extracts of SOA formed by oxidation of isoprene, α-pinene, α-terpineol and toluene. We observed substantial formation of free radicals including •OH, superoxide (HO_2•), and organic radicals (R•/RO•) upon irradiation. Compared to dark conditions, the radical yield was enhanced by a factor of ~30 for •OH, by a factor of 2-10 for superoxide radicals, and we observed the emergence of organic radicals. Total peroxide measurements showed substantial decreases of peroxide contents after photoirradiation, indicating that organic peroxides can be an important source of the observed radicals. Liquid chromatography interface with high-resolution mass spectrometry was used to detect a number of organic radicals in the form of adducts with a spin trap, BMPO. The types of detected radicals and aqueous photolysis of model compounds indicated that photolysis of carbonyls by Norrish type I mechanism plays an important role in the organic radical formation. The photolytic ROS formation serves as the driving force for cloud and fog processing of SOA.

INTRODUCTION

Secondary organic aerosols (SOA) contribute to the burden of atmospheric particulate matter (PM), playing a critical role in aerosol effects on climate, air quality and public health.[1,2] SOA originate from oxidation of anthropogenic and biogenic volatile organic compounds (VOCs), followed by nucleation and condensation of oxidation products into the particle phase.[3] SOA can undergo various aging processes, including reactive uptake of oxidants and heterogeneous oxidation, aqueous-phase processing in cloud and fog droplets,[4,5] and a suite of condensed-phase reactions such as photolysis, hydrolysis, and other particle-phase reactions.[6–8] Photochemistry is a main driver of many atmospheric aging processes, either indirectly by supplying gas-phase free radicals that can react with SOA particles, or more directly by initiating condensed-phase photochemical reactions leading to the transformation or removal of SOA compounds. While the heterogeneous reactions between gaseous oxidants and various organic surfaces have been studied extensively,[9] the aging of SOA driven by condensed-phase photochemistry (e.g., for SOA compounds dissolved in cloud droplets) has received less attention, posing challenges to evaluating the environmental impacts of SOA.[5]

Direct photolysis reactions are initiated by a SOA compound absorbing a photon capable of splitting the molecule into two radical fragments through covalent bond cleavage.[5] The primary radicals may then produce indirect photolysis products by reacting with additional SOA compounds. The combined action of direct and indirect photolysis processes leads to chemically aged SOA. The absorption coefficients of biogenic SOA were quantified in previous studies and shown to be sufficient to sustain efficient photolysis of SOA compounds on atmospherically relevant time scales.[10–12] Irradiation of SOA with sunlight has been shown to favor photodegradation of larger SOA compounds into smaller and more volatile compounds (including CO, HCHO, HCOOH, CH_4), which can evaporate to the gas phase to cause mass loss in SOA.[6,13–

[15] Formation of new oligomeric compounds either by recombination of two free radicals or by non-radical processes has been observed as well.[16–18]

The types of free radicals produced in the photolysis of SOA compounds depend on the functional group. For example, photolysis of atmospheric carbonyls can proceed via Norrish type-I mechanism to form acyl (RC•(=O)) and alkyl (R•) radicals,[19,20] which promptly form acyl peroxy ($RC(=O)O_2$•) and alkyl peroxy radicals (RO_2•) in the presence of dissolved oxygen. Direct photolysis of organic hydroperoxides (ROOH) leads to the formation of alkoxy (RO•) and •OH radicals by breaking the weak O-O bond.[19,21] •OH radicals can unselectively react with most organic molecules, while alkoxy radicals may isomerize by an internal hydrogen atom transfer to form R(–OH)• followed by oxygen addition to form $R(–OH)O_2$•.[22,23] In addition to direct photolysis processes, free radical species can be generated though photosensitized mechanisms,[24–27] such as triplet excited states of SOA compounds abstracting a hydrogen atom or an electron from another molecule. Understanding the nuances of formation of these highly reactive free radicals is important for predicting the rate and mechanism of photochemical aging of SOA.

Direct quantification of radical formation from SOA photolysis is challenging, and only a few studies characterized ROS formation from photochemical aging of SOA. Badali et al.[28] quantified •OH radicals from photolysis of ROOH in SOA and reported a five-fold increase in rate of •OH formation compared to photolysis of H_2O_2 with equal concentrations of ROOH. Hayeck et al.[29] quantified the amount of peroxy radicals formed in irradiated films of nonanoic acid at the air-water interface. Manfrin et al.[30] characterized singlet oxygen ($^1O_2$) formation from photosensitized reactions mediated by chromophoric components in aromatic SOA, although no free radicals were directly measured. Photolytic generation of organic radicals has been shown to contribute to SOA formation.[31,32] However, systematic measurements of speciation of ROS from

SOA photolysis have not been conducted. In this study, we combined an *in-situ* UV-Vis irradiation system with electron paramagnetic resonance (EPR) spectroscopy to characterize the photolytic generation of free radicals from SOA generated by isoprene, α-terpineol, α-pinene and toluene. We measured total peroxide contents in SOA before and after photoirradiation. Liquid chromatography interfaced with electrospray ionization (ESI) high resolution mass spectrometry (HR-MS) was applied to reveal the chemical identity of organic radicals formed during SOA photolysis. We also measured radical formation by photolysis of common atmospheric carbonyls and peroxides. This study provides important insights into photoinduced aqueous-phase chemistry of SOA involving radical formation and the underlying chemical mechanism.

MATERIALS AND METHODS

Preparation of SOA. A potential aerosol mass (PAM) reactor[33] was used to generate SOA particles from •OH photooxidation of isoprene (Sigma-Aldrich, stated purity ≥ 99%), α-terpineol (Arcos Organics, ≥ 97%), α-pinene (Sigma-Aldrich, 98%), and toluene (Alfa Aesar, ≥ 99.7%). The relative humidity in the PAM reactor was 40 – 50%. While the PAM reactor applies high levels of oxidants (i.e., •OH concentration of ~ 10^{10} cm^{-3})[34] over a short reaction time, the PAM-generated SOA have similar characteristics to ambient and chamber-generated SOA in terms of mass yield, oxidation state, hygroscopicity, and chemical composition with similar mass spectra measured by a time of flight aerosol mass spectrometer (Aerodyne).[35–37] A scanning mobility particle sizer (SMPS, Grimm Aerosol Technik) was used to record the particle size distribution. SOA particles were collected on 47 mm polytetrafluoroethylene (PTFE) filters (Millipore FGLP04700, 0.2 μm pore size) for 60 – 120 min with average filter mass loadings over four samples of 0.41 ± 0.08 mg, 1.03 ± 0.23 mg, 0.64 ± 0.21 mg and 2.18 ± 0.56 mg for isoprene, α-

terpineol, α-pinene, and toluene SOA, respectively. The filter samples were extracted into 1 mL of 10 mM aqueous solutions containing spin trap 5-*tert*-butoxycarbonyl-5-methyl-1-pyrroline-N-oxide (BMPO) (Enzo Life Sciences, ≥99%) by agitation for 7 min. The filters after extraction were dried under nitrogen flow for 10 – 20 min. The filter mass difference before and after the extraction was considered as the amount of SOA dissolved in the solution, and an average molar mass of 200 g mol^{-1} [38] was assumed to calculate the effective SOA molar concentrations in filter extracts. SOA concentrations were in the range of 1.7 – 2.5 mM, 4.0 – 6.3 mM, 2.3 – 4.3 mM, and 8.1 – 13.7 mM for isoprene, α-terpineol, α-pinene, and toluene SOA, respectively.

We performed additional experiments with α-pinene SOA generated a 5 m^3 Teflon chamber at ~40% RH and ~23 °C. Approximately 200 ppb of α-pinene and 2 ppm of H_2O_2 were added to the chamber by injecting measured volumes of pure α-pinene and 40% solution of H_2O_2 into a flask and evaporating them into a gently heated air flow going into the chamber. A bank of UV-B lights centered at 310 nm produced •OH in the chamber by photolysis of H_2O_2 resulting in steady-state •OH concentrations of the order of ~ 10^7 cm^{-3}. The particle size distribution was measured using a TSI model 3936 SMPS. After 2 h of irradiation, SOA was collected onto PTFE filters (Millipore, 0.2 μm pore size) with a flow rate of about 20 L min^{-1} for about 2 h with an average mass loading of 1.06±0.17 mg.

EPR Analysis. A continuous-wave electron paramagnetic resonance (CW-EPR) spectrometer (Bruker, Germany) coupled with a spin-trapping technique was used to quantify the free radical formation in the aqueous phase. The free radicals were captured by a spin-trapping agent BMPO. After particle extraction into 1 mL of aqueous 10 mM BMPO solutions, a 50 μL aliquot of the SOA extract was loaded into a 50 μL capillary tube (VWR) and inserted in the resonator of the EPR spectrometer for temporal measurements over 75 min. To characterize the

radical formation upon UV irradiation, an *in-situ* UV irradiation system (ER203UV, Bruker, Germany) equipped with a 100 W Hg lamp was used with EPR. The lamp was warmed up for ~10 min before the start of any irradiation experiments. A safety shutter between the lamp and the resonator was used to control the start and stop of irradiation. A liquid light guide focused the light to the EPR resonator where samples were exposed to broadband radiation with a wavelength range of 300 – 600 nm (the spectral flux density incident on the samples is shown in Fig. S1). The sample was extracted as described above and immediately loaded onto the EPR. For the time-dependent measurements, the background spectrum was recorded during ~ 3 min after placing the sample in the resonator, and the shutter was then raised to initiate photochemistry. The measurements were then conducted every 3 min for 75 min in total to monitor the change of BMPO-radical concentrations over time. The radical yield was calculated by normalizing the concentrations of BMPO adducts to starting effective concentration of SOA compounds in the aqueous extracts. This yield represents a cumulative yield of radicals building up during irradiation with a caveat that BMPO adducts themselves decay in time, both spontaneously and as a result of photochemical reactions in solution.[39]

In addition to SOA, the ROS formation from different model compounds was also characterized under the same irradiation conditions including *t*-butyl peroxy benzoate (Sigma Aldrich, 98%), *t*-butyl hydroperoxide (Sigma Aldrich, 70% in water), cumene hydroperoxide (Alfa Aesar, 80%), and *cis*-pinonic acid (Sigma Aldrich 98%). The concentrations were 1 mM for peroxides (*t*-butyl peroxy benzoate, *t*-butyl hydroperoxide, cumene hydroperoxide) and 10 mM for pinonic acid, respectively.

The operating parameters for EPR measurements were as follows: a center field of 3515.0 G, a sweep width of 100.0 G, a receiver gain of 30 dB, a modulation amplitude of 1.0 G, a scan

number of 10 – 20, attenuation of 12 dB, a microwave power of 12.6 mW, a modulation frequency of 100 kHz, a microwave frequency of 9.86 GHz and a conversion time and time constant of 5.12 ms. After obtaining the EPR spectra, SpinFit and SpinCount methods embedded in the Bruker Xenon software were applied to quantify BMPO-radical adducts at each time point.[38]

Total peroxide measurement. The total peroxide measurements were conducted using a modified iodometric-spectrophotometric method.[40] Peroxides in all forms can oxidize I^- to form I_2, which combines with the excess I^- to form I_3^- with characteristic absorbance peaks at wavelengths 289 nm and 350 nm[41] and the absorbance at 350 nm was measured in this study. Isoprene, α-terpineol and toluene SOA were dissolved by vortex extraction in 1 mL Milli-Q water for 7 min. The SOA extracts were divided into three groups which were measured directly after extraction, 75 min after irradiation and 75 min under dark conditions, respectively. For the irradiated samples, 200 μL of aqueous SOA extracts were placed in a glass tube and then inserted into the EPR resonator. Unlike with the EPR samples irradiated in the capillary tubes, the entire volume fits within the resonator. The sample was then irradiated for 75 min. As a control group, the rest of SOA extracts were left under dark conditions for 75 min, after which the peroxide fractions were measured together with the irradiated sample.

To conduct the assay, 100 μL of the SOA extracts from three groups were mixed with 700 μL ethyl acetate (Sigma-Aldrich, 99.8%) to obtain 800 μL diluted extracts. Then the 800 μL diluted extracts were mixed with 1200 μL reagents consisting of 636 μL acetic acid (Sigma-Aldrich, ≥ 99%), 324 μL chloroform (Sigma-Aldrich, ≥ 99.5%) and 240 μL water (acetic acid:chloroform:water = v:v 0.53:0.27:0.20). Note that the dilution factor of SOA extracts in the reagents (i.e., 100 μL of SOA in 2000 μL of reagent) was determined when different reagents were completely miscible so that the solution was homogeneous. The 2000 μL diluted SOA extracts

with reagents were then purged with a flow of 15 cm^3 min^{-1} N_2 for 1 min to exclude dissolved oxygen that can also slowly oxidize I^-. Next, 20 mg of solid potassium iodide (KI, Sigma-Aldrich, ≥ 99%) was dissolved into each sample, after which the vials were capped and allowed to stand for 1 h. Lastly, the solution was further diluted in water by a factor of 200 (25 μL of SOA in 5000 μL reagent) and the absorbance at 350 nm was measured using an online miniature spectrophotometer (Ocean Optics). The calibration was performed using 0.2 – 2 μM benzoyl peroxide (Sigma-Aldrich, ≥ 98%). Blank (water instead of SOA extracts or benzoyl peroxide) correction was always performed, and the measurements were repeated twice for each SOA sample.

High-Resolution Mass Spectrometry Analysis. Prior to mass spectrometry analysis, a filter containing ~ 0.47 mg of SOA was extracted into 1.0 mL of water. The extract was divided into four 200 μL samples with different conditions as follows: no UV irradiation without BMPO addition, UV irradiation without BMPO, no UV irradiation with 10 mM BMPO dissolved into the solution, and UV irradiation with 10 mM BMPO. The UV samples were irradiated by the same setup as described in the EPR analysis section for 75 min. The aqueous solutions were further diluted by adding acetonitrile and water as needed to reach a final solvent mixture of 50:50 v:v ACN: water with a final concentration of ~ 0.4 g L^{-1} BMPO and then loaded into the mass spectrometer.

Changes in the chemical composition of organic radicals formed upon SOA photolysis were characterized by high resolution mass spectrometry, as described in previous work[8] and in the SI. The instrument was a Thermo Scientific Vanquish Horizon ultra-performance liquid chromatography (UPLC) System coupled to a Thermo Scientific Q Exactive Plus Orbitrap high-resolution mass spectrometer with a heated electrospray ionization (HESI) source. The UPLC retention time data were not directly used in this analysis – all chromatograms were integrated

with respect to the retention time to get a full mass spectrum. Nevertheless, the separation is useful because it is expected to reduce matrix effects (i.e., suppression of ionization of less ionizable compounds) for the complex mixture of SOA and BMPO.

The chromatograms were integrated between 1 and 16 min in Thermo Scientific program FreeStyle 1.6 and then *m/z* values and abundances were determined using the Decon2LS program (https://omics.pnl.gov/software/decontoolsdecon2ls). Peaks due to ^{13}C compounds and peaks that were present in the blank at the same or greater intensity as the samples were discarded. The peaks were assigned with 0.001 *m/z* accuracy to formulas [$C_xH_yO_zN_{0-2}$]. Unassigned peaks were removed along with peaks containing more than one nitrogen as the samples were generated under NO_x free conditions and samples adducted with BMPO are expected to only contain one nitrogen atom (this primarily affected minor peaks).

RESULTS AND DISCUSSION

Photolytic generation of free radicals in aqueous solutions containing SOA. Time evolution of radical formation was characterized using the EPR-spin trap method from photolysis of isoprene, α-terpineol, α-pinene and toluene SOA. Figure 1 shows the temporal evolution of EPR spectra of BMPO-radical adducts from isoprene SOA photolysis. At reaction time $t = 0$ min before the Hg lamp is switched on, the EPR spectrum is almost flat showing negligible radical formation in the absence of irradiation. The spectrum at $t = 3.1$ min represents the first measurement after the light is switched on, showing superoxide formation with minor contributions from •OH and organic radicals. The $O_2^{\bullet -}$ keeps increasing through the second measurement ($t = 6.2$ min), while carbon- and oxygen-centered organic radicals take over after 15.4 min and reach maximum at ~ 46.0 min. The spectra at $t = 46.0$ min and $t = 76.6$ min are very similar, indicating a plateau is

reached after t = 46.0 min especially for carbon- and oxygen-centered organic radicals which dominate the radical formation. The deconvolution and simulations of EPR spectra (Fig. S2) allows us to quantify the time evolution of yields of different radicals, as shown in Fig. 2. Note that the EPR spectra for α-pinene SOA generated by the PAM chamber and the environmental chamber are very similar with negligible spectral differences (Fig. S3), indicating that the SOA generation method does not substantially affect ROS formation. We conducted control experiments under dark conditions without irradiation, showing that •OH and superoxide radicals were formed in the timescale of ~30 min, as consistent with our previous studies.[38,39,42] Note that although no organic radicals are quantified under dark conditions as they are not differentiable above instrument noise (Fig. S4), they may be present in very low concentrations.

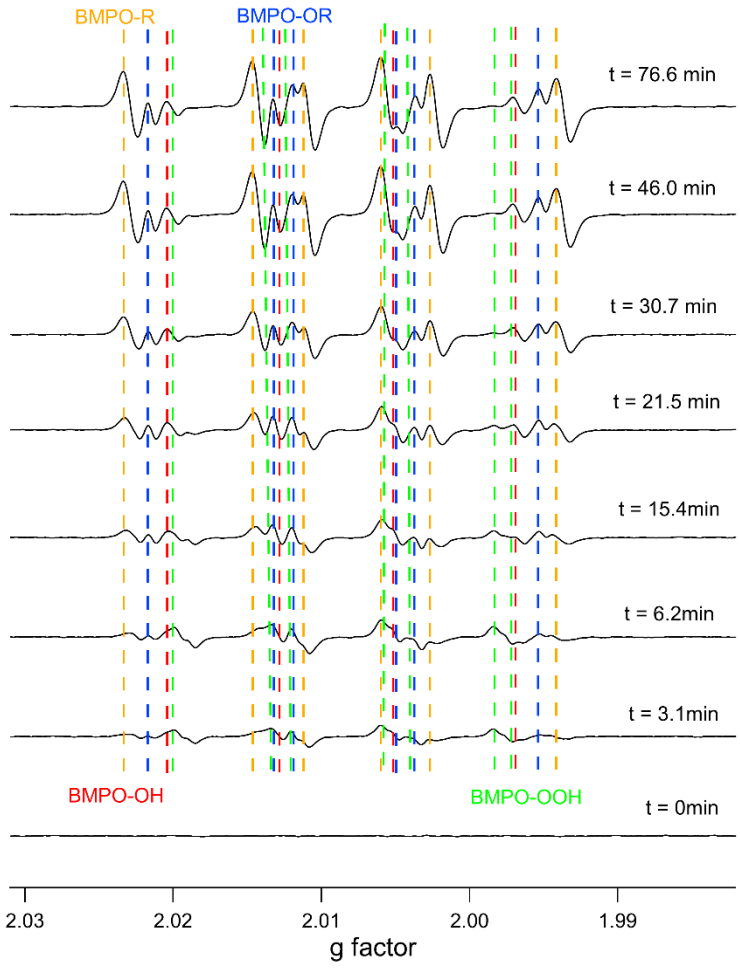

Figure 1. Time evolution of EPR spectra of BMPO-radical adducts from isoprene SOA with *in-situ* irradiation over 76.6 min. The dashed vertical lines represent different BMPO-radical adducts including BMPO-OH (red), BMPO-OOH (green), BMPO-R (orange), and BMPO-OR (blue). The measurements were taken every 3.1 min, but only 8 spectra are selected to show prominent changes over 76.6 min.

In addition to isoprene SOA, we characterized free radical formation from α-terpineol, α-pinene and toluene SOA under irradiated versus dark conditions, and the time evolution of radical yields are shown in Fig. 2. The radical formation under dark conditions (open markers) increased gradually with superoxide as the dominant radical species for all types of SOA reaching radical yields of ~0.01-0.03% with minor contributions from •OH in isoprene SOA (~0.004% yield). All SOA show substantial formation of organic radicals upon irradiation (solid squares), with radical yields (i.e., BMPO adduct concentrations normalized to the effective starting concentration of SOA compounds) from 0.02 – 1.2% for oxygen centered and carbon centered organic radicals combined. The total organic radical yield is the highest for isoprene SOA reaching ~1.2%, followed by α-terpineol SOA (~ 0.7%), α-pinene SOA (~0.6%) and toluene SOA (~0.02%). The much lower yield for toluene SOA is qualitatively consistent with previous observations of lower photodegradation rates of SOA derived from •OH oxidation of an aromatic precursor (trimethylbenzene) compared to SOA from isoprene and α-pinene.[10] Compared to dark conditions, UV-Vis irradiation significantly enhances the radical formation by a factor of ~30 for •OH in isoprene SOA and OOH by a factor of ~10 in toluene SOA and a factor of 2-5 for the biogenic SOA. For all types of SOA, an initial increase of $O_2^{\bullet -}$ formation is consistently observed, which decreases within 10 – 20 min of irradiation. The sharp decrease within 20 min can be due to the self-decomposition as well as the direct photolysis of BMPO-OOH adducts as shown in our recent study.[39] Note that the substantial formation of carbon-centered radicals indicates efficient trapping by BMPO, outcompeting the reaction between R• + O_2 for the formation of oxygen-centered

organic radicals. Under atmospheric conditions we expect the carbon centered radicals to mostly react with dissolved O_2, but the use of BMPO enables the identification of first-generation radicals and provides interesting mechanistic insight into the photochemical aging of SOA. Interestingly, biogenic SOA upon irradiation consistently showed a steep increase in organic radical formation within ~20 min. In contrast, organic radical formation from toluene SOA (Fig. 3d) shows moderate to negligible increase over 75 min. Overall, the organic radical formation plateaus within 75 min, indicating that the maximum capacity of radical formation from the dissolved SOA compounds has been reached and the sinks (such as self-decomposition, isomerization, and photolysis) of BMPO-organic-radical adducts become more important beyond one hour of photochemistry.

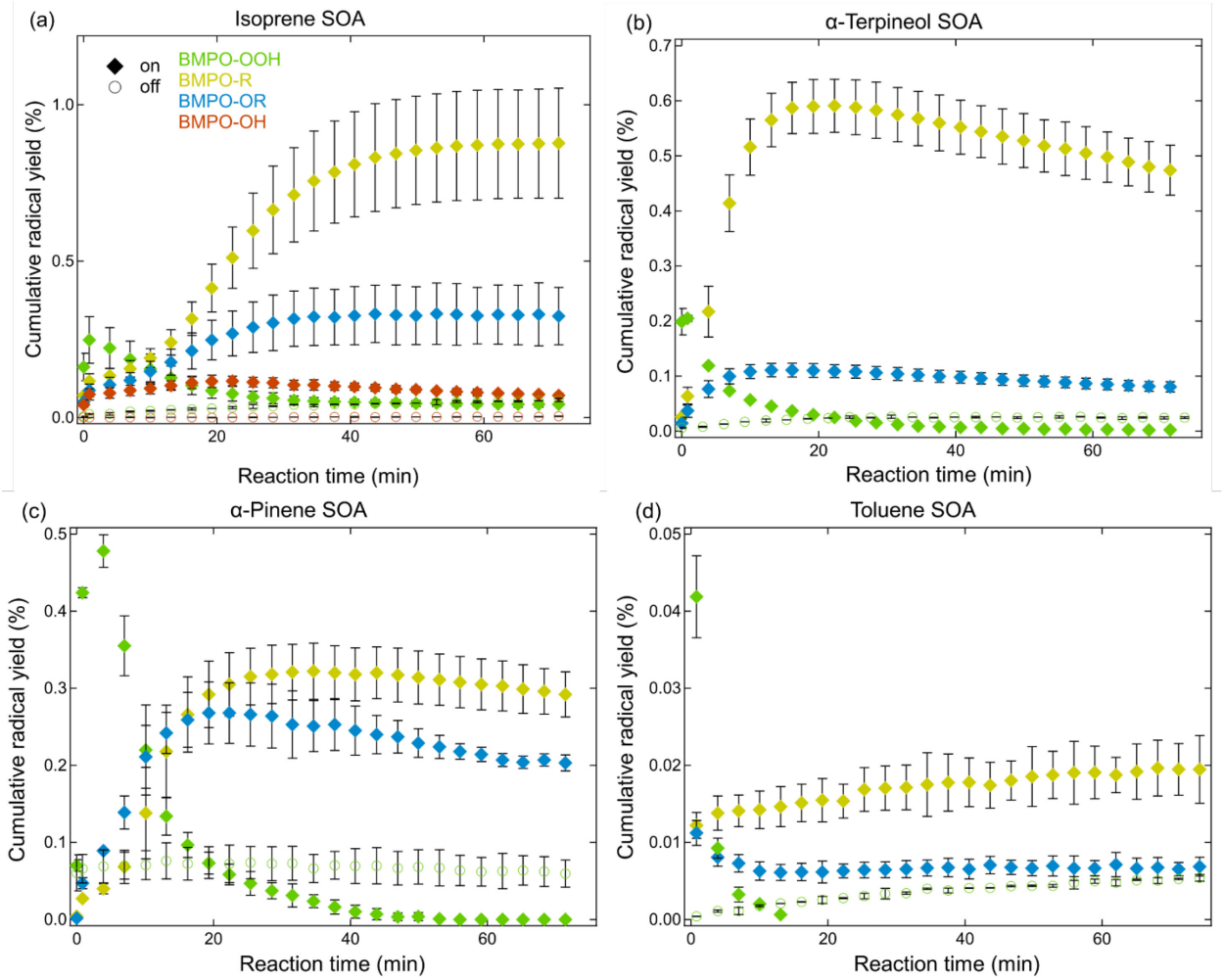

Figure 2. Temporal formation of BMPO-radical adducts from (a) isoprene, (b) α-terpineol, (c) α-pinene and (d) toluene SOA under UV-Vis irradiation ("on", solid squares) versus dark conditions ("off", open circles). Different BMPO-radical adducts are color-coded including BMPO-OH (red), BMPO-OOH (green), BMPO-R (yellow), and BMPO-OR (blue). The error bars represent the error propagation from the two duplicate SOA samples with the uncertainty in SOA mass measurements.

Total peroxide fractions. Given the high quantum yields of direct photolysis of organic hydroperoxides,[43] we performed total peroxide measurements for isoprene, α-terpineol and toluene SOA as shown in Fig. 3. The peroxide fractions (ratio of molar concentrations of [peroxide]/[SOA]) in the original extracts were 101±16%, 47±29% and 21±5% for isoprene, α-terpineol and toluene SOA, respectively, as consistent with our recent study.[44] After 75 min in dark conditions, the peroxide fraction for isoprene SOA decreased negligibly although peroxide fraction for α-terpineol and toluene SOA decreased notably to about 27±23% and 12±2.1%, respectively. Upon irradiation, the peroxide fractions further decrease to 52±24%, 18±9%, and 5.1±1.7% for isoprene, α-terpineol and toluene SOA, respectively, equivalent to 50 – 75% decrease from the total peroxide fractions in the original extracts, which is consistent with the labile nature of peroxide photolysis.[14,21] The photolysis of ROOH should lead to simultaneous formation of RO• with •OH.[28] RO• can undergo rapid isomerization or β-scission to generate R•,[45] which potentially explains the dominant R• formation over RO• as shown in Fig. 2(a)-(d). These results provide a strong correlation between the decomposition of organic peroxides and radical production during irradiation of SOA.

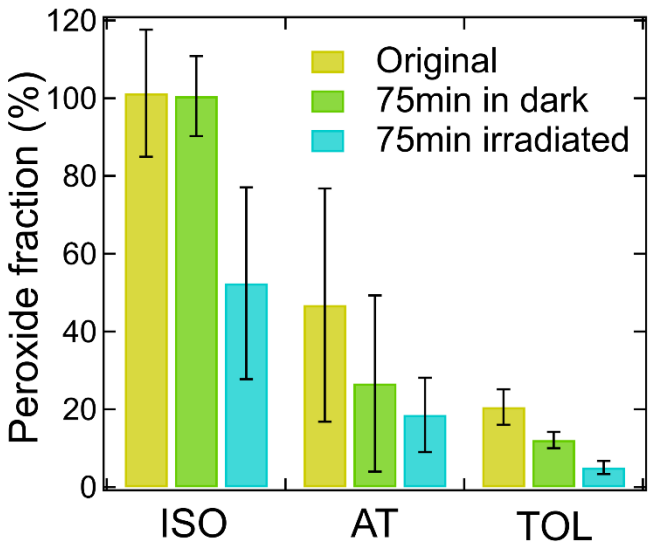

Figure 3. Total peroxide molar fractions from isoprene (ISO), α-terpineol (AT) and toluene (TOL) SOA in original extracts, 75 min under dark conditions and 75 min under UV-Vis irradiation. The error bars represent the error propagation from the two duplicate SOA samples in peroxide measurements with the uncertainty in SOA mass measurements.

Composition of organic radicals in α-pinene SOA. Although EPR data provide relevant information about *in-situ* radical formation, EPR is unable to speciate organic radicals. To address this limitation, we analyzed the composition of α-pinene SOA generated under dark and irradiated conditions with and without BMPO using UPLC-ESI-HRMS. It was recently demonstrated[38,46] that BMPO and its adducts are readily detectable in ESI, although their ionization mechanisms are more complex compared to closed-shell compounds. Figure S5 shows the full normalized mass spectra collected from *m/z* 100-700 for the dark and irradiated samples with the dominant peaks in both samples appearing at *m/z* 200.129, 399.250, and 144.066, corresponding to protonated BMPO, $[BMPO+H]^+$, BMPO cluster ion, $[BMPO+BMPO+H]^+$, and protonated BMPO fragment, $[BMPO-C_4H_8+H]^+$, respectively. The dominance of the unadducted BMPO peaks reflects the excess BMPO added to the solution to create a pseudo first order trapping reaction and minimize the effects of BMPO concentration on the trapping.

To emphasize the BMPO adducts, Fig. 4 shows the difference in normalized relative abundance between the dark and irradiated sample between *m/z* 200-400, and major adducts are identified in Table 1. The $[BMPO+H]^+$ and $[BMPO+BMPO+H]^+$ peaks at *m/z* 200.129 and 399.250 decrease in abundance after irradiation, which is consistent with the expected consumption of BMPO by trapped radicals.

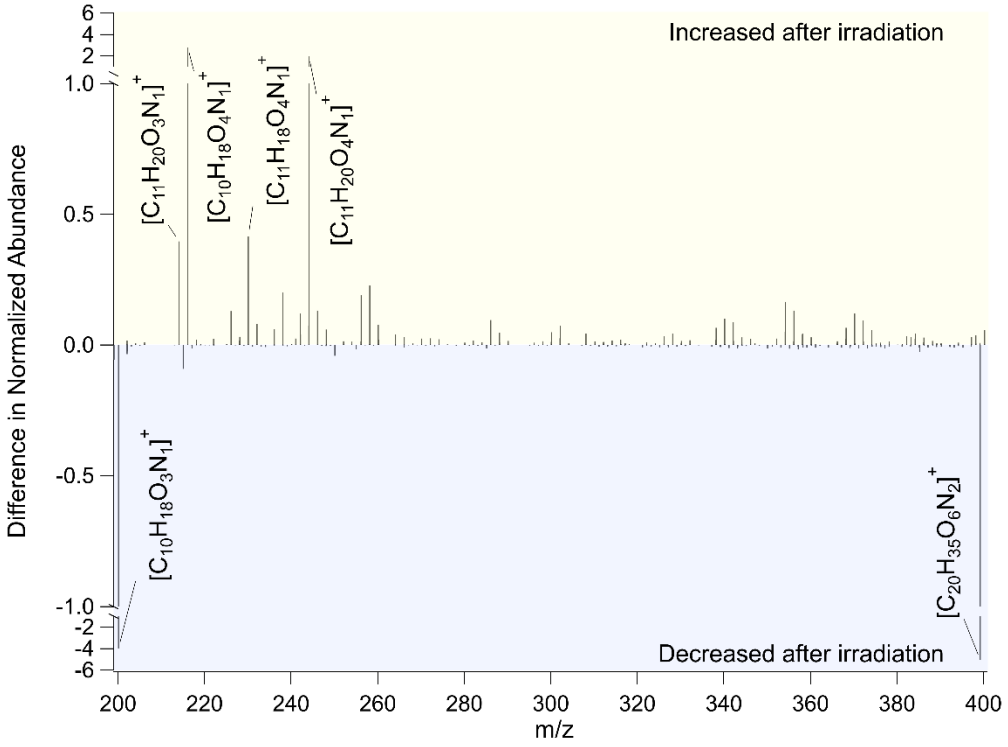

Figure 4. Difference in the normalized relative abundance of the positive ion mode mass spectra before and after irradiation of the α-pinene + BMPO solution. The major peaks from left to right correspond to *m/z* 200.129, 214.144, 216.123, 230.140, 244.154, and 399.250, respectively.

Table 1: Summary of observed BMPO adducts in irradiated α-pinene SOA extract.

BMPO adduct	***m/z* value(s)**	**Formula(s)**	**Detected ion(s)**	**Fractional abundances**$^+$
BMPO	200.129	$C_{10}H_{18}O_3N_1^+$	$[BMPO+H]^+$	40.23

BMPO–CH_3	214.144	$C_{11}H_{20}O_3N_1^+$	$[BMPO+CH_3]^+$	0.40
	216.160	$C_{11}H_{22}O_3N_1^+$	$[BMPO+CH_3+2H]^+$	0.06
BMPO–OH	216.123	$C_{10}H_{18}O_4N_1^+$	$[BMPO+OH]^+$	3.07
	218.139	$C_{10}H_{20}O_4N_1^+$	$[BMPO+OH+2H]^+$	0.07
BMPO–CHO	228.123	$C_{11}H_{18}O_4N_1^+$	$[BMPO+CHO]^+$	0.02
	230.140	$C_{11}H_{20}O_4N_1^+$	$[BMPO+CHO+2H]^+$	0.43
BMPO–CH_3O	230.140	$C_{11}H_{20}O_4N_1^+$	$[BMPO+CH_3O]^+$	0.43
	232.154	$C_{11}H_{22}O_4N_1^+$	$[BMPO+CH_3O+2H]^+$	0.09
BMPO–HO_2	232.118	$C_{10}H_{18}O_5N_1^+$	$[BMPO+HO_2]^+$	0.08
	234.134	$C_{10}H_{20}O_5N_1^+$	$[BMPO+HO_2+2H]^+$	0.06
BMPO–C_2H_3O	242.139	$C_{12}H_{20}O_4N_1^+$	$[BMPO+C_2H_3O]^+$	0.14
	244.154	$C_{12}H_{22}O_4N_1^+$	$[BMPO+C_2H_3O+2H]^+$	2.00
BMPO–COOH	244.118	$C_{11}H_{18}O_5N_1^+$	$[BMPO+COOH]^+$	0.08
	246.134	$C_{11}H_{20}O_5N_1^+$	$[BMPO+COOH+2H]^+$	0.15
BMPO–$C_2H_3O_2$	258.134	$C_{12}H_{20}O_5N_1^+$	$[BMPO+C_2H_3O_2]^+$	0.01
	260.149	$C_{12}H_{22}O_5N_1^+$	$[BMPO+C_2H_3O_2+2H]^+$	0.09
BMPO–$C_6H_9O_2$	312.181	$C_{16}H_{26}O_5N_1^+$	$[BMPO+C_6H_9O_2]^+$	0.05
	314.196	$C_{16}H_{28}O_5N_1^+$	$[BMPO+C_6H_9O_2+2H]^+$	0.06
BMPO–$C_8H_{13}O$	324.217	$C_{18}H_{30}O_4N_1^+$	$[BMPO+C_8H_{13}O]^+$	0.13
	326.233	$C_{18}H_{32}O_4N_1^+$	$[BMPO+C_8H_{13}O+2H]^+$	0.01
BMPO–$C_8H_{11}O_2$	338.196	$C_{18}H_{28}O_5N_1^+$	$[BMPO+C_8H_{11}O_2]^+$	0.02
	340.212	$C_{18}H_{30}O_5N_1^+$	$[BMPO+C_8H_{11}O_2+2H]^+$	0.10
BMPO–$C_9H_{15}O$	338.233	$C_{19}H_{32}O_4N_1^+$	$[BMPO+C_9H_{15}O]^+$	0.07

	340.248	$C_{19}H_{34}O_4N_1^+$	$[BMPO+C_9H_{15}O+2H]^+$	0.01
BMPO–$C_7H_9O_3$	340.175	$C_{17}H_{26}O_6N_1^+$	$[BMPO+C_7H_9O_3]^+$	0.02
	342.191	$C_{17}H_{26}O_6N_1^+$	$[BMPO+C_7H_9O_3+2H]^+$	0.09
BMPO–$C_8H_{13}O_2$	340.212	$C_{18}H_{30}O_5N_1^+$	$[BMPO+C_8H_{13}O_2]^+$	0.10
	342.227	$C_{18}H_{32}O_5N_1^+$	$[BMPO+C_8H_{13}O_2+2H]^+$	0.03
BMPO–$C_7H_{13}O_3$	344.207	$C_{17}H_{30}O_6N_1^+$	$[BMPO+C_7H_{13}O_3]^+$	0.07
	346.222	$C_{17}H_{32}O_6N_1^+$	$[BMPO+C_7H_{13}O_3+2H]^+$	0.02
BMPO–$C_9H_{13}O_2$	352.212	$C_{19}H_{30}O_5N_1^+$	$[BMPO+C_9H_{13}O_2]^+$	0.02
	354.227	$C_{19}H_{32}O_5N_1^+$	$[BMPO+C_9H_{13}O_2+2H]^+$	0.17
BMPO–$C_9H_{15}O_2$	354.227	$C_{19}H_{32}O_5N_1^+$	$[BMPO+C_9H_{15}O_2]^+$	0.17
	356.243	$C_{19}H_{34}O_5N_1^+$	$[BMPO+C_9H_{15}O_2+2H]^+$	0.03
BMPO–$C_8H_{13}O_3$	356.207	$C_{18}H_{30}O_6N_1^+$	$[BMPO+C_8H_{13}O_3]^+$	0.14
	358.222	$C_{18}H_{32}O_6N_1^+$	$[BMPO+C_8H_{13}O_3+2H]^+$	0.06
BMPO–$C_9H_{11}O_3$	nd	$C_{19}H_{28}O_6N_1^+$	$[BMPO+C_9H_{11}O_3]^+$	nd
	368.207	$C_{19}H_{30}O_6N_1^+$	$[BMPO+C_9H_{11}O_3+2H]^+$	0.03
BMPO–$C_{10}H_{15}O_2$	366.228	$C_{20}H_{32}O_5N_1^+$	$[BMPO+C_{10}H_{15}O_2]^+$	0.02
	368.243	$C_{20}H_{34}O_5N_1^+$	$[BMPO+C_{10}H_{15}O_2+2H]^+$	0.07
BMPO–$C_8H_9O_4$	nd	$C_{18}H_{26}O_7N_1^+$	$[BMPO+C_8H_9O_4]^+$	nd
	370.186	$C_{18}H_{28}O_7N_1^+$	$[BMPO+C_8H_9O_4+2H]^+$	0.02
BMPO–$C_9H_{13}O_3$	368.207	$C_{19}H_{30}O_6N_1^+$	$[BMPO+C_9H_{13}O_3]^+$	0.03
	370.222	$C_{19}H_{32}O_6N_1^+$	$[BMPO+C_9H_{13}O_3+2H]^+$	0.13
BMPO–$C_8H_{13}O_4$	372.202	$C_{18}H_{30}O_7N_1^+$	$[BMPO+C_8H_{13}O_4]^+$	0.10
	374.217	$C_{18}H_{32}O_7N_1^+$	$[BMPO+C_8H_{13}O_4+2H]^+$	0.08

BMPO–$C_{10}H_{15}O_3$	382.222	$C_{20}H_{32}O_6N_1^+$	$[BMPO+C_{10}H_{15}O_3]^+$	0.04
	384.238	$C_{20}H_{34}O_6N_1^+$	$[BMPO+C_{10}H_{15}O_3+2H]^+$	0.09
BMPO–$C_9H_{13}O_4$	384.202	$C_{19}H_{30}O_7N_1^+$	$[BMPO+C_9H_{13}O_4]^+$	0.02
	386.217	$C_{19}H_{32}O_7N_1^+$	$[BMPO+C_9H_{13}O_4+2H]^+$	0.04
BMPO Cluster	399.250	$C_{20}H_{35}O_6N_2^+$	$[BMPO+BMPO+H]^+$	5.08
BMPO–$C_9H_{13}O_5$	400.197	$C_{19}H_{30}O_8N_1^+$	$[BMPO+C_9H_{13}O_5]^+$	0.02
	402.212	$C_{19}H_{32}O_8N_1^+$	$[BMPO+C_9H_{13}O_5+2H]^+$	0.02

┼ Relative abundance of the irradiated sample normalized to the total abundance.

The mass spectrometry data of the BMPO radical adducts formed after irradiation identifies chemical formulas of the radicals observed using EPR, providing new insights into the processes responsible for their formation. As shown in Fig. 4 and Table 1, BMPO–OH is the most prominent adduct after photolysis of α-pinene SOA (detected as $[BMPO+OH]^+$ at *m/z* 216.123). This is not fully consistent with the EPR results which were dominated by BMPO-OOH. A possible reason for this apparent discrepancy is that BMPO-OH adduct may have a higher ionization efficiency than BMPO-OOH adduct (detected as $[BMPO+HO_2]^+$ at *m/z* 232.118). Another possible explanation is that BMPO-OOH might decompose into BMPO-OH, as previously described for DMPO.[47,48] Note that BMPO-OOH is known to be more stable than DMPO-OOH,[49] and we have not observed the decomposition of BMPO-OOH into BMPO-OH during EPR measurements in previous studies,[42,50] but we cannot rule out potential decomposition in the ion source upon HR-MS analysis. This highlights the challenge of quantifying radical adducts by mass spectrometry due to the uncertainty introduced by the complex ionization processes. Therefore, we will rely on mass spectrometry for qualitative radical identification rather than for quantification in this work.

The BMPO radical adducts identified using mass spectrometry can be used to support the presence of some of the dominant SOA direct photolysis pathways. In order to propose fragmentation mechanisms, potential precursor molecules were identified by comparing the irradiated and non-irradiated samples without BMPO in both positive and negative ion mode, shown in Fig. S6 and S7, respectively. The process for proposing photolysis pathways is further discussed in the SI. As previously described,[46] BMPO-radical adducts can ionize via two main pathways, one producing an $[M]^+$ ion and the other producing an $[M + 2H]^+$ ion (Table 1). For this reason, both pathways were considered when identifying the photolysis products that could contribute to the BMPO adduct signals. The pathways responsible for producing the dominant BMPO adduct signals at *m/z* 214.144, 230.140, and 244.154 in Fig. 4 are discussed below along with select products from oxopinonaldehyde photolysis (Fig. S8). The BMPO adducts of all the other radical products proposed in the SI mechanisms and their relative abundances are listed in Table 1.

The largest increase in abundance for a BMPO adduct with an organic radical was for a peak at *m/z* 244.154 with a formula of $C_{12}H_{22}O_4N^+$, which can either be interpreted as the $[M]^+$ ionization of BMPO-C_2H_5O or the $[M+2H]^+$ ionization of BMPO-C_2H_3O. None of the fragmentation products identified in the SI directly produce a C_2H_5O radical, while the C_2H_3O can result from the Norrish type I splitting of any compound terminated with an acetyl (-C(=O)CH_3) group, which is common for α-pinene oxidation products compounds 3, 6, and 6a (Fig. S10, S13, and S14). The plethora of photolysis pathways that produce C_2H_3O, coupled with the absence of any explanation for direct C_2H_5O production, suggest that C_2H_3O is primarily responsible for the peak at *m/z* 244.154.

The second largest increase for an organic radical adduct appeared for the peak at *m/z* 230.140 with a corresponding formula of $C_{11}H_{20}O_4N^+$, which could either correspond to the $[M]^+$ ionization of BMPO-CH_3O adduct or the $[M+2H]^+$ ionization of a BMPO-CHO adduct. Both radicals can be expected as CH_3O can be produced via photolysis of compound 4 in Fig. S11, and CHO can be produced via the fragmentation of compounds shown in Fig. S8, 9, 13, and 14 (compounds 1, 2, 6, and 6a). We can tentatively conclude that both CHO and CH_3O radicals contribute to the peak at *m/z* 230.140 and are both present in the sample.

The next most significant increase in organic BMPO adduct is observed at *m/z* 214.144 with a formula $C_{11}H_{20}O_3N^+$, which can be assigned to corresponds to $[M]^+$ ionization of the BMPO-CH_3 adduct. Unlike the previous two peaks, this assignment is less ambiguous as there are no known ways to produce CH radical in photolysis of α-pinene SOA compounds. Based on the mechanisms for the precursors explored in the SI, the CH_3 radical can be formed through the photolysis of compounds 1, 6, and 6a shown in Fig. S8, S13, and S14. These radicals detected by mass spectrometry offer chemical formulas for the organic radical adducts detected by EPR, but they do not offer any structural information about the adducts. The CH_3 radical can only contribute to the BMPO-R EPR signal, although CHO and C_2H_3O can resonate between both carbon centered and oxygen centered radicals, providing a likely source for some of the BMPO-OR signal shown in Fig. 2.

The mass spectrometry results listed in Table 1 can also be used to identify several BMPO-adducts corresponding to the larger fragments produced by the photolysis pathways described in Fig. S8-14. Unlike the three organic radicals discussed in this section, most of these larger radicals are only produced by one or two photolysis pathways, providing more concrete evidence for the occurrence of individual pathways. For example, Fig. S8 shows the radical products from the

Norrish type I photolysis of oxopinonaldehyde across the ketones producing several pairs of organic radicals: $C_9H_{13}O_2$ and CHO and $C_9H_{11}O_3$ and CH_3, discussed below, as well as $C_8H_{13}O$ and C_2HO_2 and $C_8H_{11}O_2$ and C_2H_3O, discussed in the SI.

The BMPO adduct for $C_9H_{13}O_2$ is detected as both $[M]^+$ and the more prominent $[M+2H]^+$ at *m/z* 352.212 and 354.227, respectively, while the CHO adduct was detected prominently as an $[M+2H]^+$ adduct, as previously discussed. The detection of both radicals is consistent with the photolysis mechanism in Fig. S8.

The $C_9H_{11}O_3$ radical is also detected as a BMPO adduct at *m/z* 368.207 for $[M+2H]^+$, however there is no signal at *m/z* 366.192, the anticipated *m/z* for the $[M]^+$ adduct. Additionally, the *m/z* 368.207 also corresponds to the $[M]^+$ BMPO adduct with $C_9H_{13}O_3$, which can also be produced via photolysis of compounds 2, 4, and 5. This suggests it is unlikely that this photolysis pathway is contributing significantly to the radical formation detected in the solution. This could be because the other radical produced via this pathway, CH_3, is a small, unstable radical, making it relatively less favorable than the resonance stabilized radicals produced by the other photolysis pathways of this compound.

The mass spectrometry results offer molecular identification of the organic radical adducts detected using EPR and provide insights into the photolysis mechanisms occurring within the sample. The mass spectrometry results also suggest the aging of α-pinene SOA is a significant source for acyl radicals, which have an important role in atmospheric chemistry as precursors for highly oxygenated organic molecules (HOMs) and acylperoxynitrates.[51–54]

ROS formation from model compounds. To further explore potential sources for the radical formation from irradiated SOA, different model compounds and their mixtures were

characterized under similar photoirradiation conditions, including *t*-butyl peroxy benzoate, *t*-butyl hydroperoxide, cumene hydroperoxide, and *cis*-pinonic acid (Fig. S15).

As shown in Fig. 5, immediately after irradiation, (a) cumene hydroperoxide, (b) *t*-butyl hydroperoxide, (c) pinonic acid, and (d) *t*-butyl peroxy benzoate formed a variety of radicals, including superoxide, hydroxyl, and carbon-centered radicals, in line with the signal observed for the SOA samples. However, the peroxide photolysis did not produce any detectable oxygen-centered organic radical, which would form in photolysis of the weakest O-O bonds in these molecules. This apparent lack of RO radicals could be due to the interconversion between oxygen- and carbon-centered organic radicals via aqueous isomerization,[55] decomposition, or H-abstraction.[44,56] This suggests that the type of organic radical detected is also influenced by radical stability. No hydroxyl radical was observed upon photolysis of cumene hydroperoxide, suggesting that this radical breaks into R• + HO_2• instead of RO• + •OH due the resonance stabilization of the tertiary benzylic radical produced via C-O bond cleavage. The comparison of radical population for SOA and peroxides suggests that peroxide photolysis is not solely responsible for the radical production during SOA irradiation. By contrast, pinonic acid, a ubiquitous α-pinene SOA product, formed both carbon- and oxygen-centered organic radicals upon irradiation in addition to superoxide. This result confirms that photolysis of carbonyls can be a major source of oxygen-centered radicals, consistent with previous studies.[20,57]

Although mass spectrometry does not provide structural information about the adducts, the formulas can provide possible explanations for the appearance of both BMPO-R and BMPO-OR EPR signals. Based on the predicted photolysis pathways, only the peroxide photolysis in Fig. S10 and S13 resulted in oxygen centered radicals, but the direct photolysis of peroxides in aqueous solutions produced no detectable BMPO-OR signal. This suggests that the other organic radicals

detected via HRMS contribute to the BMPO-OR signal. Many of the carbon-centered radicals predicted via Norrish type I photolysis appear on the carbon of a carbonyl, which can readily undergo keto-enol tautomerization to produce an oxygen centered radical.[58] This also explains the oxygen- and carbon-centered radicals produced during the irradiation of pinonic acid, further supporting that the photolysis of carbonyls is likely responsible for the oxygen-centered radicals detected by EPR. Pinonic acid also contains a carboxylic acid functional group, but carboxylic acids are not known to undergo photolysis at the wavelengths used in this study.[59] Future experiments using a wider variety of model carbonyl-containing compounds should be conducted to gain further insight into the role of carbonyls in radical formation during irradiation.

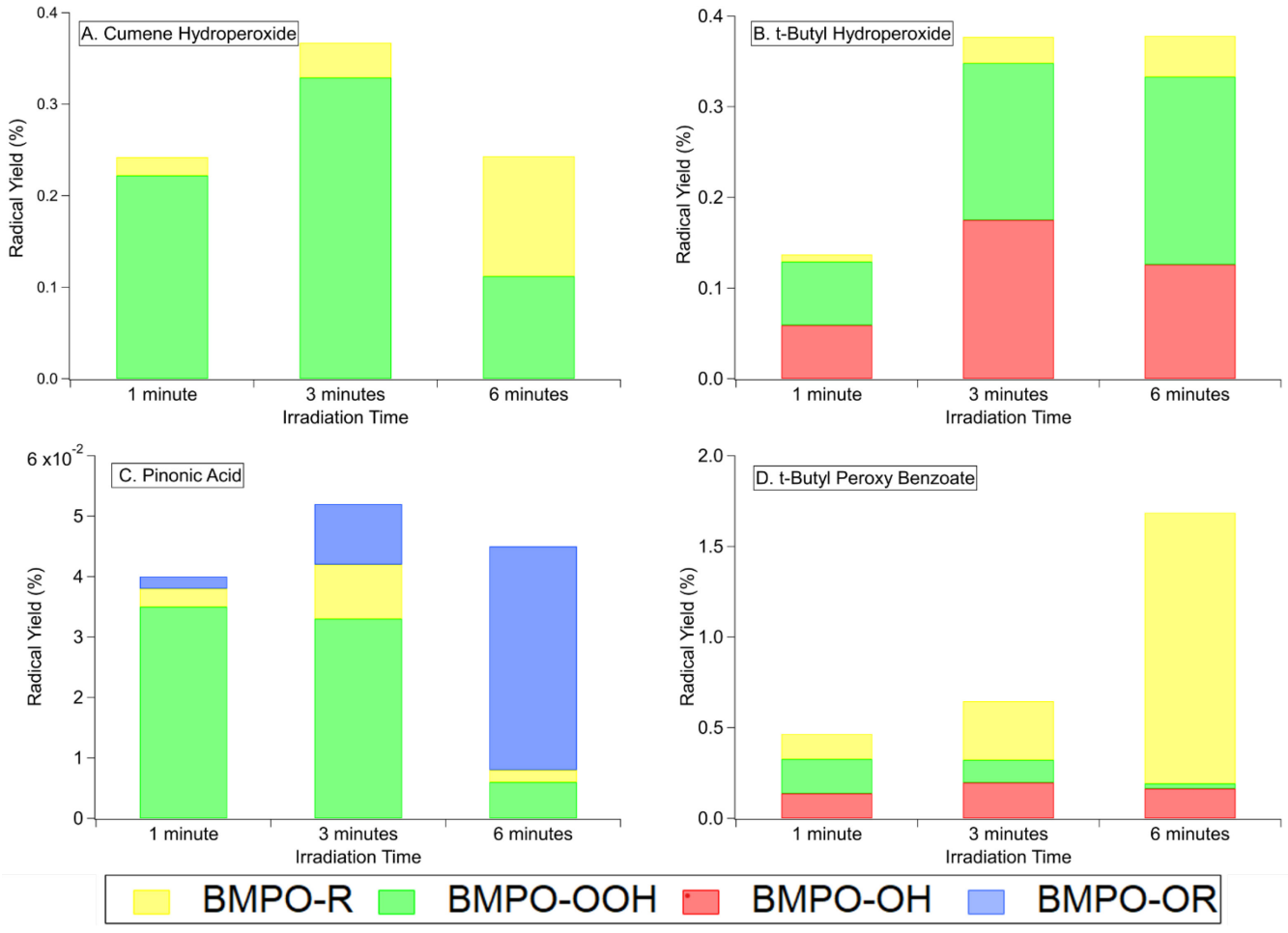

Figure 5. Radical yields by (a) 1 mM cumene hydroperoxide, (b) 1 mM *t*-butyl hydroperoxide (c) 10 mM pinonic acid, and (d) 1 mM *t*-butyl peroxy benzoate under UV-Vis irradiation.

Atmospheric Implications. In this study, we combined an *in-situ* UV-Vis irradiation system with EPR to characterize the photolytic formation of ROS from laboratory-generated SOA. Substantial radical formation is observed upon irradiation for isoprene, α-pinene, α-terpineol, and toluene SOA, with enhancement factors of up to ~30 for •OH radicals and up to ~10 for superoxide radicals, compared to dark conditions as well as the emergence of organic radicals. Using total peroxide measurements and model peroxide EPR results, we observed that photolysis of peroxide and carbonyl compounds provide an aqueous source of ROS. The formation of ROS induces radical chain reactions and oxidative aging in the condensed phase, which may alter the climatic and toxicological properties of the particles.[60,61]

The results from high-resolution mass spectrometry provide chemical formulas for the organic radicals formed during the photochemical aging of α-pinene SOA, identifying C_2H_3O, CHO, and CH_3 as the most abundant organic radicals. They also suggest that carbonyl photolysis is a major source of organic radicals during α-pinene irradiation, producing a multitude of acyl radicals (•R=O). These acyl radicals may serve as precursors for the formation of atmospheric esters and other highly oxygenated organic molecules,[51–53,62] which affect SOA loading in the atmosphere. Acyl radicals can also undergo O_2 addition to form acyl-peroxy radicals that can react in the presence of NO_2 to form acylperoxynitrates, which represent an important atmospheric reservoir for NO_x.[54]

This work identifies organic peroxides and carbonyls as important sources of ROS and organic radicals during the photochemical aging of SOA. Future work should explore the

mechanisms responsible for radical formation in SOA and explore the role of other functional groups in atmospheric photochemical aging.

ASSOCIATED CONTENT

The Supporting Information is available free of charge at [insert DOI].

Contains 15 supporting figures and 2 supporting tables, as well as additional information on mass spectrometry operating parameters, spectral flux density for irradiation set up, EPR spectra for SOA and model compounds, mass spectra for α-pinene SOA, SOA photolysis precursor identification and photolysis pathways.

AUTHOR INFORMATION

Corresponding Authors

- Manabu Shiraiwa - Department of Chemistry, University of California, Irvine, Irvine, California 92697, United States; https://orcid.org/0000-0003-2532-5373; Email: m.shiraiwa@uci.edu
- Sergey A. Nizkorodov - Department of Chemistry, University of California, Irvine, Irvine, California 92697, United States; https://orcid.org/0000-0003-0891-0052; Email: nizkorod@uci.edu

Authors

- Lena Gerritz - Department of Chemistry, University of California, Irvine, California 92697-2025, United States, https://orcid.org/0009-0009-9971-1526
- Jinlai Wei - Department of Chemistry, University of California, Irvine, Irvine, California 92697, United States; https://orcid.org/0000-0002-4741-9015
- Ting Fang - Department of Chemistry, University of California, Irvine, Irvine, California 92697, United States; https://orcid.org/0000-0002-4845-2749
- Cynthia Wong - Department of Chemistry, University of California, Irvine, California 92697-2025, United States; https://orcid.org/0000-0002-1597-6861
- Alexandra L. Klodt - Department of Chemistry, University of California, Irvine, Irvine, California 92697, United States; https://orcid.org/0000-0002-3558-972X

Author Contributions

The experiments and data analysis were conceived by M.S. and S.A.N. EPR and HRMS experiments were done by J.W. and L.G. Data analysis was done by J.W. and L.G., with help from T.F., C.W., and A.L.K.. The manuscript was started by J.W. and finished by L.G. All authors have participated in editing and approved the final version of the manuscript.

Notes. The authors declare no financial competing interests.

ACKNOWLEDGEMENTS

We acknowledge funding from the National Science Foundation (CHE-2203419, CHE-1808125). We thank Prof. William Brune (Pennsylvania State University) for loaning the PAM reactor. L.G thanks the NSF GRFP program for supporting her research.

REFERENCES.

(1) Jimenez, J. L.; Canagaratna, M. R.; Donahue, N. M.; Prevot, A. S. H.; Zhang, Q.; Kroll, J. H.; DeCarlo, P. F.; Allan, J. D.; Coe, H.; Ng, N. L.; Aiken, A. C.; Docherty, K. S.; Ulbrich, I. M.; Grieshop, A. P.; Robinson, A. L.; Duplissy, J.; Smith, J. D.; Wilson, K. R.; Lanz, V. A.; Hueglin, C.; Sun, Y. L.; Tian, J.; Laaksonen, A.; Raatikainen, T.; Rautiainen, J.; Vaattovaara, P.; Ehn, M.; Kulmala, M.; Tomlinson, J. M.; Collins, D. R.; Cubison, M. J.; Dunlea, E. J.; Huffman, J. A.; Onasch, T. B.; Alfarra, M. R.; Williams, P. I.; Bower, K.; Kondo, Y.; Schneider, J.; Drewnick, F.; Borrmann, S.; Weimer, S.; Demerjian, K.; Salcedo, D.; Cottrell, L.; Griffin, R.; Takami, A.; Miyoshi, T.; Hatakeyama, S.; Shimono, A.; Sun, J. Y.; Zhang, Y. M.; Dzepina, K.; Kimmel, J. R.; Sueper, D.; Jayne, J. T.; Herndon, S. C.; Trimborn, A. M.; Williams, L. R.; Wood, E. C.; Middlebrook, A. M.; Kolb, C. E.; Baltensperger, U.; Worsnop, D. R. Evolution of Organic Aerosols in the Atmosphere. *Science* **2009**, *326* (5959), 1525–1529. https://doi.org/10.1126/science.1180353.

(2) Shiraiwa, M.; Ueda, K.; Pozzer, A.; Lammel, G.; Kampf, C. J.; Fushimi, A.; Enami, S.; Arangio, A. M.; Frohlich-Nowoisky, J.; Fujitani, Y.; Furuyama, A.; Lakey, P. S. J.; Lelieveld, J.; Lucas, K.; Morino, Y.; Poschl, U.; Takaharna, S.; Takami, A.; Tong, H. J.; Weber, B.; Yoshino, A.; Sato, K. Aerosol Health Effects from Molecular to Global Scales. *Environ Sci Technol* **2017**, *51* (23), 13545–13567. https://doi.org/10.1021/acs.est.7b04417.

(3) Ziemann, P. J.; Atkinson, R. Kinetics, Products, and Mechanisms of Secondary Organic Aerosol Formation. *Chemical Society Reviews* **2012**, *41* (19), 6582–6605. https://doi.org/10.1039/C2CS35122F.

(4) Rudich, Y.; Donahue, N. M.; Mentel, T. F. Aging of Organic Aerosol: Bridging the Gap Between Laboratory and Field Studies. *Annual Review of Physical Chemistry* **2007**, *58* (1), 321–352. https://doi.org/10.1146/annurev.physchem.58.032806.104432.

(5) George, C.; Ammann, M.; D'Anna, B.; Donaldson, D. J.; Nizkorodov, S. A. Heterogeneous Photochemistry in the Atmosphere. *Chemical Reviews* **2015**, *115* (10), 4218–4258. https://doi.org/10.1021/cr500648z.

(6) Baboomian, V. J.; Gu, Y.; Nizkorodov, S. A. Photodegradation of Secondary Organic Aerosols by Long-Term Exposure to Solar Actinic Radiation. *ACS Earth and Space Chemistry* **2020**, *4* (7), 1078–1089. https://doi.org/10.1021/acsearthspacechem.0c00088.

(7) Donahue, N. M.; Robinson, A. L.; Trump, E. R.; Riipinen, I.; Kroll, J. H. Volatility and Aging of Atmospheric Organic Aerosol. In *Atmospheric and Aerosol Chemistry*; McNeill, V. F., Ariya, P. A., Eds.; Springer Berlin Heidelberg: Berlin, Heidelberg, 2012; pp 97–143. https://doi.org/10.1007/128_2012_355.

(8) Klodt, A. L.; Romonosky, D. E.; Lin, P.; Laskin, J.; Laskin, A.; Nizkorodov, S. A. Aqueous Photochemistry of Secondary Organic Aerosol of α-Pinene and α-Humulene in the Presence of Hydrogen Peroxide or Inorganic Salts. *ACS Earth Space Chem.* **2019**, *3* (12), 2736–2746. https://doi.org/10.1021/acsearthspacechem.9b00222.

(9) Abbatt, J. P. D.; Lee, A. K. Y.; Thornton, J. A. Quantifying Trace Gas Uptake to Tropospheric Aerosol: Recent Advances and Remaining Challenges. *Chemical Society Reviews* **2012**, *41* (19), 6555–6581.

(10) Malecha, K. T.; Nizkorodov, S. A. Photodegradation of Secondary Organic Aerosol Particles as a Source of Small, Oxygenated Volatile Organic Compounds. *Environ. Sci. Technol.* **2016**, *50* (18), 9990–9997. https://doi.org/10.1021/acs.est.6b02313.

(11) Romonosky, D. E.; Ali, N. N.; Saiduddin, M. N.; Wu, M.; Lee, H. J. (Julie); Aiona, P. K.; Nizkorodov, S. A. Effective Absorption Cross Sections and Photolysis Rates of Anthropogenic and Biogenic Secondary Organic Aerosols. *Atmospheric Environment* **2016**, *130*, 172–179. https://doi.org/10.1016/j.atmosenv.2015.10.019.

(12) Zawadowicz, M. A.; Lee, B. H.; Shrivastava, M.; Zelenyuk, A.; Zaveri, R. A.; Flynn, C.; Thornton, J. A.; Shilling, J. E. Photolysis Controls Atmospheric Budgets of Biogenic Secondary Organic Aerosol. *Environ. Sci. Technol.* **2020**, *54* (7), 3861–3870. https://doi.org/10.1021/acs.est.9b07051.

(13) Malecha, K. T.; Cai, Z.; Nizkorodov, S. A. Photodegradation of Secondary Organic Aerosol Material Quantified with a Quartz Crystal Microbalance. *Environ. Sci. Technol. Lett.* **2018**, *5* (6), 366–371. https://doi.org/10.1021/acs.estlett.8b00231.

(14) Epstein, S. A.; Blair, S. L.; Nizkorodov, S. A. Direct Photolysis of α-Pinene Ozonolysis Secondary Organic Aerosol: Effect on Particle Mass and Peroxide Content. *Environ. Sci. Technol.* **2014**, *48* (19), 11251–11258. https://doi.org/10.1021/es502350u.

(15) Henry, K. M.; Donahue, N. M. Photochemical Aging of α-Pinene Secondary Organic Aerosol: Effects of OH Radical Sources and Photolysis. *The Journal of Physical Chemistry A* **2012**, *116* (24), 5932–5940. https://doi.org/10.1021/jp210288s.

(16) Baboomian, V. J.; Crescenzo, G. V.; Huang, Y.; Mahrt, F.; Shiraiwa, M.; Bertram, A. K.; Nizkorodov, S. A. Sunlight Can Convert Atmospheric Aerosols into a Glassy Solid State and Modify Their

Environmental Impacts. *Proc. Natl. Acad. Sci. U.S.A.* **2022**, *119* (43), e2208121119. https://doi.org/10.1073/pnas.2208121119.

(17) Rapf, R. J.; Perkins, R. J.; Dooley, M. R.; Kroll, J. A.; Carpenter, B. K.; Vaida, V. Environmental Processing of Lipids Driven by Aqueous Photochemistry of α-Keto Acids. *ACS Cent. Sci.* **2018**, *4* (5), 624–630. https://doi.org/10.1021/acscentsci.8b00124.

(18) Walhout, E. Q.; Yu, H.; Thrasher, C.; Shusterman, J. M.; O'Brien, R. E. Effects of Photolysis on the Chemical and Optical Properties of Secondary Organic Material Over Extended Time Scales. *ACS Earth Space Chem.* **2019**, *3* (7), 1226–1236. https://doi.org/10.1021/acsearthspacechem.9b00109.

(19) Bateman, A. P.; Nizkorodov, S. A.; Laskin, J.; Laskin, A. Photolytic Processing of Secondary Organic Aerosols Dissolved in Cloud Droplets. *Phys Chem Chem Phys* **2011**, *13* (26), 12199–12212. https://doi.org/10.1039/c1cp20526a.

(20) Mang, S. A.; Henricksen, D. K.; Bateman, A. P.; Andersen, M. P. S.; Blake, D. R.; Nizkorodov, S. A. Contribution of Carbonyl Photochemistry to Aging of Atmospheric Secondary Organic Aerosol. *J. Phys. Chem. A* **2008**, *112* (36), 8337–8344. https://doi.org/10.1021/jp804376c.

(21) Krapf, M.; El Haddad, I.; Bruns, E. A.; Molteni, U.; Daellenbach, K. R.; Prevot, A. S. H.; Baltensperger, U.; Dommen, J. Labile Peroxides in Secondary Organic Aerosol. *Chem* **2016**, *1* (4), 603–616. https://doi.org/10.1016/j.chempr.2016.09.007.

(22) Monod, A.; Chevallier, E.; Durand Jolibois, R.; Doussin, J. F.; Picquet-Varrault, B.; Carlier, P. Photooxidation of Methylhydroperoxide and Ethylhydroperoxide in the Aqueous Phase under Simulated Cloud Droplet Conditions. *Atmospheric Environment* **2007**, *41* (11), 2412–2426. https://doi.org/10.1016/j.atmosenv.2006.10.006.

(23) Atkinson, R. Rate Constants for the Atmospheric Reactions of Alkoxy Radicals: An Updated Estimation Method. *Atmospheric Environment* **2007**, *41* (38), 8468–8485. https://doi.org/10.1016/j.atmosenv.2007.07.002.

(24) Li, F.; Zhou, S.; Du, L.; Zhao, J.; Hang, J.; Wang, X. Aqueous-Phase Chemistry of Atmospheric Phenolic Compounds: A Critical Review of Laboratory Studies. *Science of The Total Environment* **2023**, *856*, 158895. https://doi.org/10.1016/j.scitotenv.2022.158895.

(25) Vione, D.; Maurino, V.; Minero, C.; Pelizzetti, E.; Harrison, M. A. J.; Olariu, R.-I.; Arsene, C. Photochemical Reactions in the Tropospheric Aqueous Phase and on Particulate Matter. *Chem. Soc. Rev.* **2006**, 10.1039.b510796m. https://doi.org/10.1039/b510796m.

(26) Corral Arroyo, P.; Bartels-Rausch, T.; Alpert, P. A.; Dumas, S.; Perrier, S.; George, C.; Ammann, M. Particle-Phase Photosensitized Radical Production and Aerosol Aging. *Environ. Sci. Technol.* **2018**, *52* (14), 7680–7688. https://doi.org/10.1021/acs.est.8b00329.

(27) Rossignol, S.; Aregahegn, K. Z.; Tinel, L.; Fine, L.; Nozière, B.; George, C. Glyoxal Induced Atmospheric Photosensitized Chemistry Leading to Organic Aerosol Growth. *Environ. Sci. Technol.* **2014**, *48* (6), 3218–3227. https://doi.org/10.1021/es405581g.

(28) Badali, K. M.; Zhou, S.; Aljawhary, D.; Antiñolo, M.; Chen, W. J.; Lok, A.; Mungall, E.; Wong, J. P. S.; Zhao, R.; Abbatt, J. P. D. *Formation of Hydroxyl Radicals from Photolysis of Secondary Organic Aerosol*

Material; Aerosols/Laboratory Studies/Troposphere/Chemistry (chemical composition and reactions), 2015. https://doi.org/10.5194/acpd-15-4117-2015.

(29) Hayeck, N.; Mussa, I.; Perrier, S.; George, C. Production of Peroxy Radicals from the Photochemical Reaction of Fatty Acids at the Air–Water Interface. *ACS Earth Space Chem.* **2020**, *4* (8), 1247–1253. https://doi.org/10.1021/acsearthspacechem.0c00048.

(30) Manfrin, A.; Nizkorodov, S. A.; Malecha, K. T.; Getzinger, G. J.; McNeill, K.; Borduas-Dedekind, N. Reactive Oxygen Species Production from Secondary Organic Aerosols: The Importance of Singlet Oxygen. *Environ. Sci. Technol.* **2019**, *53* (15), 8553–8562. https://doi.org/10.1021/acs.est.9b01609.

(31) Kessler, S. H.; Nah, T.; Carrasquillo, A. J.; Jayne, J. T.; Worsnop, D. R.; Wilson, K. R.; Kroll, J. H. Formation of Secondary Organic Aerosol from the Direct Photolytic Generation of Organic Radicals. *The Journal of Physical Chemistry Letters* **2011**, *2* (11), 1295–1300. https://doi.org/10.1021/jz200432n.

(32) Healy, R. M.; Chen, Y.; Kourtchev, I.; Kalberer, M.; O'Shea, D.; Wenger, J. C. Rapid Formation of Secondary Organic Aerosol from the Photolysis of 1-Nitronaphthalene: Role of Naphthoxy Radical Self-Reaction. *Environmental Science & Technology* **2012**, *46* (21), 11813–11820. https://doi.org/10.1021/es302841j.

(33) Kang, E.; Root, M. J.; Toohey, D. W.; Brune, W. H. Introducing the Concept of Potential Aerosol Mass (PAM). *Atmos. Chem. Phys.* **2007**, *7* (22), 5727–5744. https://doi.org/10.5194/acp-7-5727-2007.

(34) Kang, E.; Toohey, D. W.; Brune, W. H. Dependence of SOA Oxidation on Organic Aerosol Mass Concentration and OH Exposure: Experimental PAM Chamber Studies. *Atmos Chem Phys* **2011**, *11* (4), 1837–1852. https://doi.org/10.5194/acp-11-1837-2011.

(35) Lambe, A. T.; Chhabra, P. S.; Onasch, T. B.; Brune, W. H.; Hunter, J. F.; Kroll, J. H.; Cummings, M. J.; Brogan, J. F.; Parmar, Y.; Worsnop, D. R.; Kolb, C. E.; Davidovits, P. Effect of Oxidant Concentration, Exposure Time, and Seed Particles on Secondary Organic Aerosol Chemical Composition and Yield. *Atmos Chem Phys* **2015**, *15* (6), 3063–3075. https://doi.org/10.5194/acp-15-3063-2015.

(36) Lambe, A. T.; Ahern, A. T.; Williams, L. R.; Slowik, J. G.; Wong, J. P. S.; Abbatt, J. P. D.; Brune, W. H.; Ng, N. L.; Wright, J. P.; Croasdale, D. R.; Worsnop, D. R.; Davidovits, P.; Onasch, T. B. Characterization of Aerosol Photooxidation Flow Reactors: Heterogeneous Oxidation, Secondary Organic Aerosol Formation and Cloud Condensation Nuclei Activity Measurements. *Atmos. Meas. Tech.* **2011**, *4* (3), 445–461. https://doi.org/10.5194/amt-4-445-2011.

(37) Peng, Z.; Jimenez, J. L. Radical Chemistry in Oxidation Flow Reactors for Atmospheric Chemistry Research. *Chemical Society Reviews* **2020**, *49* (9), 2570–2616. https://doi.org/10.1039/C9CS00766K.

(38) Tong, H.; Arangio, A. M.; Lakey, P. S. J.; Berkemeier, T.; Liu, F.; Kampf, C. J.; Brune, W. H.; Pöschl, U.; Shiraiwa, M. Hydroxyl Radicals from Secondary Organic Aerosol Decomposition in Water. *Atmos. Chem. Phys.* **2016**, *16* (3), 1761–1771. https://doi.org/10.5194/acp-16-1761-2016.

(39) Wei, J.; Fang, T.; Shiraiwa, M. Effects of Acidity on Reactive Oxygen Species Formation from Secondary Organic Aerosols. *ACS Environmental Au* **2022**, *2* (4), 336–345. https://doi.org/10.1021/acsenvironau.2c00018.

(40) Docherty, K. S.; Wu, W.; Lim, Y. B.; Ziemann, P. J. Contributions of Organic Peroxides to Secondary Aerosol Formed from Reactions of Monoterpenes with O3. *Environ Sci Technol* **2005**, *39* (11), 4049–4059. https://doi.org/10.1021/es050228s.

(41) Awtrey, A. D.; Connick, R. E. The Absorption Spectra of I2, I3-, I-, IO3-, S4O6= and S2O3=. Heat of the Reaction I3- = I2 + I. *Journal of the American Chemical Society* **1951**, *73* (4), 1842–1843. https://doi.org/10.1021/ja01148a504.

(42) Wei, J.; Fang, T.; Wong, C.; Lakey, P. S. J.; Nizkorodov, S. A.; Shiraiwa, M. Superoxide Formation from Aqueous Reactions of Biogenic Secondary Organic Aerosols. *Environ. Sci. Technol.* **2021**, *55* (1), 260–270. https://doi.org/10.1021/acs.est.0c07789.

(43) Epstein, S. A.; Shemesh, D.; Tran, V. T.; Nizkorodov, S. A.; Gerber, R. B. Absorption Spectra and Photolysis of Methyl Peroxide in Liquid and Frozen Water. *The Journal of Physical Chemistry A* **2012**, *116* (24), 6068–6077. https://doi.org/10.1021/jp211304v.

(44) Wei, J.; Fang, T.; Lakey, P. S. J.; Shiraiwa, M. Iron-Facilitated Organic Radical Formation from Secondary Organic Aerosols in Surrogate Lung Fluid. *Environmental Science & Technology* **2021**. https://doi.org/10.1021/acs.est.1c04334.

(45) Carrasquillo, A. J.; Daumit, K. E.; Kroll, J. H. Radical Reactivity in the Condensed Phase: Intermolecular versus Intramolecular Reactions of Alkoxy Radicals. *The Journal of Physical Chemistry Letters* **2015**, *6* (12), 2388–2392. https://doi.org/10.1021/acs.jpclett.5b00913.

(46) Gerritz, L.; Schervish, M.; Lakey, P. S. J.; Oeij, T.; Wei, J.; Nizkorodov, S. A.; Shiraiwa, M. Photoenhanced Radical Formation in Aqueous Mixtures of Levoglucosan and Benzoquinone: Implications to Photochemical Aging of Biomass-Burning Organic Aerosols. *J. Phys. Chem. A* **2023**, *127* (24), 5209–5221. https://doi.org/10.1021/acs.jpca.3c01794.

(47) Finkelstein, E.; Rosen, G. M.; Rauckman, E. J. Production of Hydroxyl Radical by Decomposition of Superoxide Spin-Trapped Adducts. *J. Mol. Pharm.* **1981**, No. 21, 262–265.

(48) Tsai, P.; Ichikawa, K.; Mailer, C.; Pou, S.; Halpern, H. J.; Robinson, B. H.; Nielsen, R.; Rosen, G. M. Esters of 5-Carboxyl-5-Methyl-1-Pyrroline *N* -Oxide: A Family of Spin Traps for Superoxide. *J. Org. Chem.* **2003**, *68* (20), 7811–7817. https://doi.org/10.1021/jo0350413.

(49) Zhao, H.; Joseph, J.; Zhang, H.; Karoui, H.; Kalyanaraman, B. Synthesis and Biochemical Applications of a Solid Cyclic Nitrone Spin Trap: A Relatively Superior Trap for Detecting Superoxide Anions and Glutathiyl Radicals. *Free Radical Biology and Medicine* **2001**, *31* (5), 599–606. https://doi.org/10.1016/S0891-5849(01)00619-0.

(50) Fang, T.; Huang, Y.-K.; Wei, J.; Monterrosa Mena, J. E.; Lakey, P. S. J.; Kleinman, M. T.; Digman, M. A.; Shiraiwa, M. Superoxide Release by Macrophages through NADPH Oxidase Activation Dominating Chemistry by Isoprene Secondary Organic Aerosols and Quinones to Cause Oxidative Damage on Membranes. *Environ. Sci. Technol.* **2022**, *56* (23), 17029–17038. https://doi.org/10.1021/acs.est.2c03987.

(51) Peräkylä, O.; Berndt, T.; Franzon, L.; Hasan, G.; Meder, M.; Valiev, R. R.; Daub, C. D.; Varelas, J. G.; Geiger, F. M.; Thomson, R. J.; Rissanen, M.; Kurtén, T.; Ehn, M. Large Gas-Phase Source of Esters and

Other Accretion Products in the Atmosphere. *J. Am. Chem. Soc.* **2023**, *145* (14), 7780–7790. https://doi.org/10.1021/jacs.2c10398.

(52) Bianchi, F.; Kurtén, T.; Riva, M.; Mohr, C.; Rissanen, M. P.; Roldin, P.; Berndt, T.; Crounse, J. D.; Wennberg, P. O.; Mentel, T. F.; Wildt, J.; Junninen, H.; Jokinen, T.; Kulmala, M.; Worsnop, D. R.; Thornton, J. A.; Donahue, N.; Kjaergaard, H. G.; Ehn, M. Highly Oxygenated Organic Molecules (HOM) from Gas-Phase Autoxidation Involving Peroxy Radicals: A Key Contributor to Atmospheric Aerosol. *Chem. Rev.* **2019**, *119* (6), 3472–3509. https://doi.org/10.1021/acs.chemrev.8b00395.

(53) Shi, X.; Tang, R.; Dong, Z.; Liu, H.; Xu, F.; Zhang, Q.; Zong, W.; Cheng, J. A Neglected Pathway for the Accretion Products Formation in the Atmosphere. *Science of The Total Environment* **2022**, *848*, 157494. https://doi.org/10.1016/j.scitotenv.2022.157494.

(54) Gaffney, J. S.; Marley, N. A. The Impacts of Peroxyacetyl Nitrate in the Atmosphere of Megacities and Large Urban Areas: A Historical Perspective. *ACS Earth Space Chem.* **2021**, *5* (8), 1829–1841. https://doi.org/10.1021/acsearthspacechem.1c00143.

(55) Schuchmann, H.-P.; Von Sonntag, C. Photolysis at 185 Nm of Dimethyl Ether in Aqueous Solution: Involvement of the Hydroxymethyl Radical. *Journal of Photochemistry* **1981**, *16* (3), 289–295. https://doi.org/10.1016/0047-2670(81)80039-1.

(56) Gilbert, B. C.; Holmes, R. G. G.; Laue, H. A. H.; Norman, R. O. C. Electron Spin Resonance Studies. Part L. Reactions of Alkoxyl Radicals Generated from Alkyl Hydroperoxides and Titanium(III) Ion in Aqueous Solution. *J. Chem. Soc., Perkin Trans. 2* **1976**, No. 9, 1047. https://doi.org/10.1039/p29760001047.

(57) Lary, D. J.; Shallcross, D. E. Central Role of Carbonyl Compounds in Atmospheric Chemistry. *J. Geophys. Res.* **2000**, *105* (D15), 19771–19778. https://doi.org/10.1029/1999JD901184.

(58) Splitter, J. S.; Calvin, M. Mechanism of the Keto-Enol Tautomerism in Radical Cations and Gas-Phase Closed-Shell Systems. *J. Am. Chem. Soc.* **1979**, *101* (24), 7329–7332. https://doi.org/10.1021/ja00518a032.

(59) Petr Klan; Jakob Wirz. Chemistry of Excited Molecules. In *Photochemistry of Organic Compounds: From Concepts to Practice*.

(60) Pöschl, U.; Shiraiwa, M. Multiphase Chemistry at the Atmosphere–Biosphere Interface Influencing Climate and Public Health in the Anthropocene. *Chem. Rev.* **2015**, *115* (10), 4440–4475. https://doi.org/10.1021/cr500487s.

(61) Wang, S.; Zhao, Y.; Chan, A. W. H.; Yao, M.; Chen, Z.; Abbatt, J. P. D. Organic Peroxides in Aerosol: Key Reactive Intermediates for Multiphase Processes in the Atmosphere. *Chem. Rev.* **2023**, *123* (4), 1635–1679. https://doi.org/10.1021/acs.chemrev.2c00430.

(62) Kenseth, C. M.; Hafeman, N. J.; Rezgui, S. P.; Chen, J.; Huang, Y.; Dalleska, N. F.; Kjaergaard, H. G.; Stoltz, B. M.; Seinfeld, J. H.; Wennberg, P. O. Particle-Phase Accretion Forms Dimer Esters in Pinene Secondary Organic Aerosol. *Science* **2023**, *382* (6672), 787–792. https://doi.org/10.1126/science.adi0857.

For Table of Contents Only.